Rogue Waves in a Multistable System

Alexander N. Pisarchik[1,*]
[1]Centro de Investigaciones en Optica, Loma del Bosque 115, 37150 Leon, Guanajuato, Mexico

Rider Jaimes-Reátegui,[2] Ricardo Sevilla-Escoboza,[2] and G. Huerta-Cuellar[2]
[2]Centro Universitario de los Lagos, Universidad de Guadalajara, Enrique Diaz de Leon 1144, Paseos de la Montaña, 47460 Lagos de Moreno, Jalisco, Mexico

Majid Taki[3]
[3]Université des Sciences et Technologies de Lille, CNRS UMR 8523-UFR de Physique-Btiment P5, 59655 Villeneuve d'Ascq Cedex, France
(Received 5 October 2011; published 29 December 2011)

Clear evidence of rogue waves in a multistable system is revealed by experiments with an erbium-doped fiber laser driven by harmonic pump modulation. The mechanism for the rogue wave formation lies in the interplay of stochastic processes with multistable deterministic dynamics. Low-frequency noise applied to a diode pump current induces rare jumps to coexisting subharmonic states with high-amplitude pulses perceived as rogue waves. The probability of these events depends on the noise filtered frequency and grows up when the noise amplitude increases. The probability distribution of spike amplitudes confirms the rogue wave character of the observed phenomenon. The results of numerical simulations are in good agreement with experiments.

DOI: 10.1103/PhysRevLett.107.274101 PACS numbers: 05.45.−a, 05.40.Ca, 42.55.Wd, 42.60.Mi

The term ''rogue wave'' was first used to talk about giant waves which emerge unexpectedly on a relatively calm ocean surface. Later, this term was extended to other fields of science, such as optics, matter physics, superfluidity, and even to economy (see, e.g., [1] and references therein), to describe rare large amplitude spikes. Although no strict definition of this phenomenon does yet exist, Akhmediev and Pelinovsky [1] suggest as many as six defining properties of rogue waves. Among them, the most significant ones are (i) a large amplitude (more than twice that of the average amplitude of the wave height), (ii) unpredictability (chaoticity), and (iii) specific shape of probability distribution function (PDF) of the wave amplitudes; some researchers point to the L-shaped PDF in a semilog scale.

Optical counterparts of oceanic freak waves have been found in a photonic crystal fiber [2] and in an optically injected semiconductor laser [3]. In the former case, optical solitons, solutions of the nonlinear Schrödinger equation are interpreted as optical rogue waves propagating along a photonic crystal fiber; rogue solitons are created because of noise amplification inherent to modulational instability. In the latter case, the giant laser pulses, referred to as rogue waves originate from fully deterministic nonlinear noise-free equations in the onset of chaos.

Depending on the matter at hand, many mechanisms have already been recognized as being responsible for rogue wave formation; among them we can distinguish modulational [4] and nonlinear spectral [5] instabilities, focusing with caustic current [6], anomalous wind excitation [7], etc. In this Letter, we suggest yet another mechanism for the rogue wave emergence, one derived from multistability. This mechanism is oblivious of the difference in size of the state basins of attraction, since a particular state is determined by initial conditions and may be changed with noise. The fact that noise induces intermittent switches between coexisting states (attractor hopping phenomenon) is well known [8,9]. When the noise amplitude is increased, the probability of these switches grows up; however, it is still unclear whether these jumps may or may not have the rogue wave properties.

Here, we study under which conditions rare giant pulses with short duration and large amplitude can appear in a multistable system. To do so, we selected a diode-pumped erbium-doped fiber laser (EDFL), because its coexisting attractors are well known [9–12]. The experimental setup is similar to that described in previous papers of some of the authors [9,10]. A 1560 nm EDFL is pumped by a 977 nm diode pump laser. The 4.81 m Fabry-Perot laser cavity is formed by an active 88 cm long heavily erbium-doped fiber with a 2.7 μm core diameter and two fiber Bragg gratings (FBGs) with 0.288 and 0.544 nm full widths on half-magnitude bandwidth, having, respectively, 100% and 95.88% reflectivities at the laser wavelength. In our experiments, the diode current is fixed at 145.5 mA corresponding to a 20 mW pump power, while the EDFL threshold occurs at 110 mA. To drive the EDFL, the sum of harmonic and random modulations, $m_d \sin(2\pi f_d t) + \eta G(\zeta, f_n)$, from signal and noise generators is applied to the diode pump current. Here, m_d and f_d are, respectively, the amplitude and frequency of the external harmonic

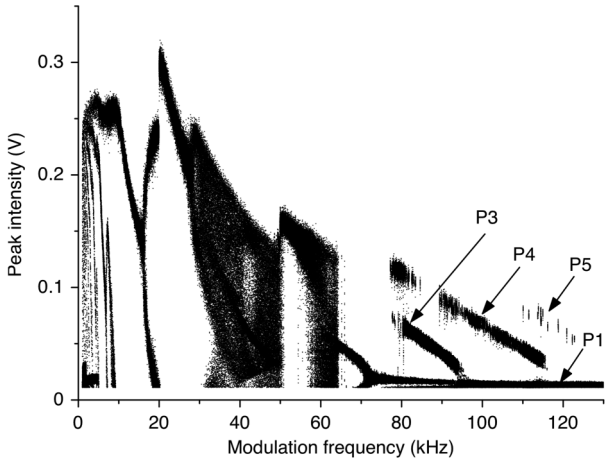

FIG. 1. Experimental bifurcation diagram of peak laser intensity versus driving frequency. The coexisting period 1 ($P1$), period 3 ($P3$), period 4 ($P4$), and period-5 ($P5$) attractors are found by switching on and off the signal generator resulting in a random change of initial conditions.

modulation, η is the noise amplitude, and $G(\zeta, f_n)$ is the zero-mean noise function in terms of a random number $\zeta \in [-1, 1]$ and the noise cutoff frequency f_n (white noise is filtered with a fifth order discrete low-pass Butterworth filter in LABVIEW 8.5). The pump current is chosen to ensure a laser relaxation oscillation frequency around $f_r = 30$ kHz. Noise with $\eta = 1$ V results in a 50% modulation depth of the pump current; both the average pump current and f_r are independent of the noise amplitude. The influence of noise on the relaxation oscillation frequency has been extensively studied in Ref. [10].

Under pump modulation, EDFL displays very rich dynamics including multistability. Figure 1 shows the experimental bifurcation diagram of the noiseless EDFL with respect to the driving frequency f_d for the driving amplitude fixed at $m_d = 0.8$ V. The diagram is obtained by recording the peak laser intensity after transients. Additional noise shifts the positions of saddle-node bifurcation points where the attractors are born and die. For relatively strong noise, the coexisting attractors lose their stability resulting in a new intermittent attractor (attractor hopping) [9].

Since we are interested in the parameter region where the laser exhibits multistability, we explore $f_d = 90$ kHz for which $P1$, $P3$, and $P4$ coexist. Figure 2 shows the experimentally observed rogue wave. The laser switches to $P4$ for only a few (3-5) periods and then falls back into the regular $P1$ regime. For the explored parameters, these events occur very rarely; the average time between the consequent rogue waves is about 30 s [13]. By varying the noise parameters f_n and η, one can control the switching probability for different coexisting states. To verify whether the observed spikes exhibit the rogue wave properties, we calculate PDFs from experimental time series obtained for different noise amplitudes (Fig. 3). The pulses with a very large intensity appear much more often than they would according to Gaussian statistics; that confirms their rogue wave character. In the presence of noise, the number of coexisting attractors changes; i.e., the multistable system is converted to a metastable one [9] where the peak intensity is not the same as it was in the noiseless system.

To model the EDFL, we use the balance equations for the intracavity laser power P and the averaged (over the active fiber length) population N of the upper level [12]:

$$\frac{dP}{dt} = \frac{2L}{T_r} P\{r_w \alpha_0 [N(\xi_1 - \xi_2) - 1] - \alpha_{\text{th}}\} + P_{\text{sp}}, \quad (1)$$

$$\frac{dN}{dt} = -\frac{\sigma_{12} r_w P}{\pi r_0^2}(N\xi_1 - 1) - \frac{N}{\tau} + P_{\text{pump}}, \quad (2)$$

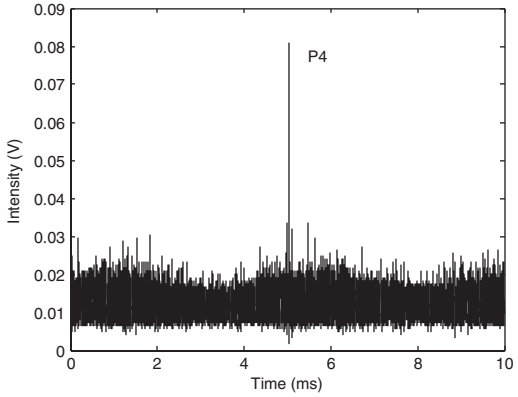

FIG. 2. Oscilloscope recording of laser oscillations demonstrating a rogue wave. Rare jumps to the period-4 states occur when loss-pass filtered noise with cutting frequency $f_n = 7$ kHz and amplitude $\eta = 0.5$ V is applied. $f_d = 90$ kHz, $m_d = 0.8$ V.

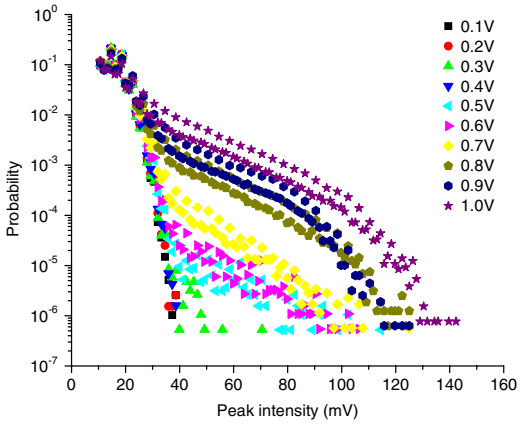

FIG. 3 (color online). Experimental probability density functions of laser peak intensity for different amplitudes of noise filtered at $f_n = 7$ kHz.

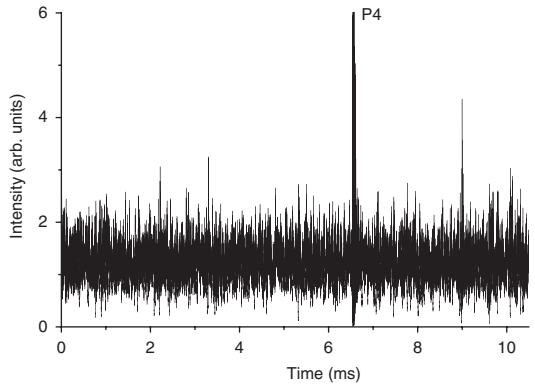

FIG. 4. Numerically calculated rogue wave of period 4 ($P4$) when noise with $f_n = 7$ kHz and $\eta = 0.9$ is applied. $f_d = 80$ kHz, $m_d = 1$.

where $N = (1/n_0 L) \int_0^L N_2(z)dz$ (N_2 being the upper level population, n_0 the refractive index of a "cold" erbium-doped fiber core, and L the active fiber length), and σ_{12} is the cross section of the absorption transition from the ground state to the upper state. Taking the cross section of the return stimulated transition σ_{21} to be practically the same as σ_{12}, we get $\xi_1 = (\sigma_{12} + \sigma_{21})/\sigma_{12} = 2$, while $\xi_2 = \sigma_{23}/\sigma_{12} = 0.4$ is the coefficient that stands for the ratio between the exited state absorption (σ_{23}) and ground-state absorption (σ_{12}) cross sections at the laser wavelength. $T_r = (2n_0/c)(L + l_0)$ is the photon intracavity round-trip time (l_0 being the total length of FBG coupler tails inside the cavity), $\alpha_0 = N_0\sigma_{12}$ is the small-signal absorption of the erbium fiber at the laser wavelength ($N_0 = N_1 + N_2$ being the total concentration of erbium ions in the active fiber). $\alpha_{\text{th}} = \gamma_0 + (1/2L) \times \ln(1/R)$ accounts for the intracavity losses on the threshold (γ_0 being the nonresonant fiber loss and R is the total reflection coefficient of the FBG couplers), τ is the lifetime of erbium ions in the excited state, r_0 is the fiber core radius, w_0 is the radius of the fundamental fiber mode, and $r_w = 1 - \exp[-2(r_0/w_0)^2]$ is the factor addressing a match between the laser fundamental mode and erbium-doped core volumes inside the active fiber. The spontaneous emission into the fundamental laser mode is derived as follows

$$P_{\text{sp}} = N \frac{10^{-3}}{\tau T_r} \left(\frac{\lambda_g}{w_0}\right)^2 \frac{r_0^2 \alpha_0 L}{4\pi^2 \sigma_{12}}, \tag{3}$$

where λ_g is the laser wavelength. The pump power is expressed as

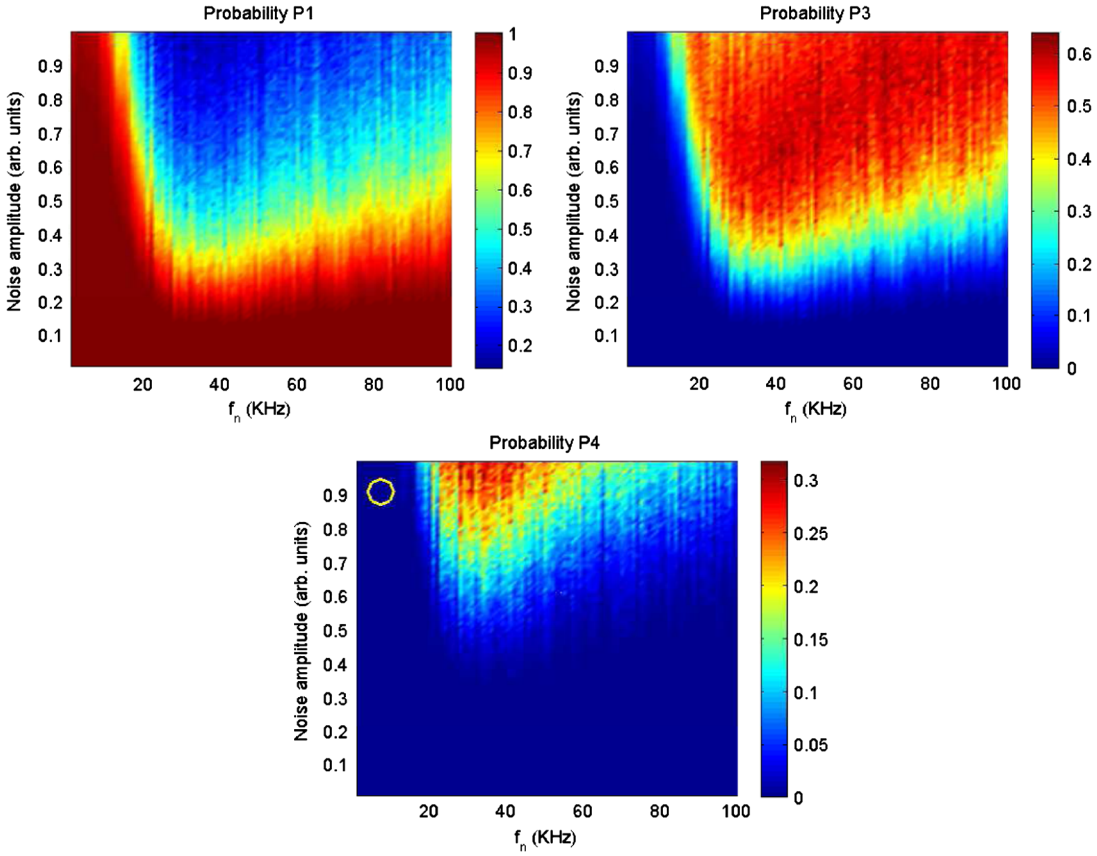

FIG. 5 (color online). Probability densities for period-1, period-3, and period-4 regimes in (f_n, η) parameter space. The circle shows the region where the rogue wave in Fig. 4 is detected.

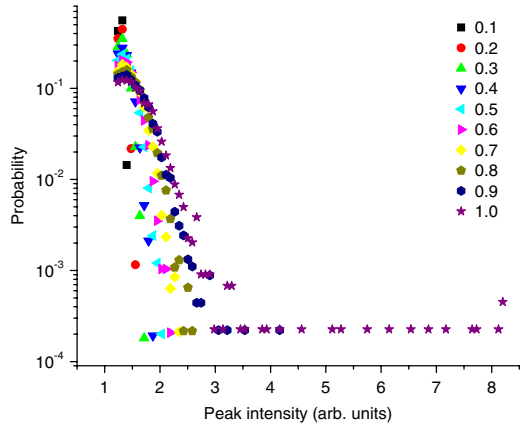

FIG. 6 (color online). Numerically calculated probability density functions of laser peak intensity for different amplitudes of noise filtered at $f_n = 7$ kHz.

$$P_{\text{pump}} = P_p \frac{1 - \exp[-\alpha_0 \beta L(1 - N)]}{N_0 \pi r_0^2 L}, \tag{4}$$

where P_p is the pump power at the fiber entrance and $\beta = \alpha_p/\alpha_0$ is a dimensionless coefficient. The coefficients characterizing the resonant-absorption properties of the EDFL at the laser and pump wavelengths are $\alpha_0 = 0.4\ \text{cm}^{-1}$ and $\beta = 0.5$. The values γ_0 and R yield $\alpha_{\text{th}} = 3.92 \times 10^{-2}$. The lasing wavelength is taken to be $\lambda_g = 1.56 \times 10^{-4}$ cm and the maximum reflection coefficients of both FBGs are centered on this wavelength. Both the harmonic modulation and noise are applied to the diode pump current as

$$P_p = p[1 - m_d \sin(2\pi f_d t) + \eta G(\zeta, f_n)], \tag{5}$$

where p is the pump power without modulation (i.e., when $m_d = 0$).

Numerical simulations are carried out with the same noise as one used in the experiments; i.e., the noise is generated in LABVIEW 8.5 and added to Eq. (5). To explore the same parameter region, the noise parameters f_n and η are varied to change the preference for different periodic states. Figure 4 shows the calculated rogue wave of $P4$ which appears with probability of about 0.0003. The probabilities for different regimes as a function of f_n and η are shown in Fig. 5. The diagrams indicate that subharmonic regimes with higher amplitudes appear more frequently as f_n approaches f_r, whereas the intermittent jumps are rare when noise is filtered for lower frequencies; the rogue waves are only observed for $f_n < f_r$ at the edge of the nonzero probability.

The calculated PDFs in Fig. 6 have a pronounced L shape in a semilog scale that justifies the rogue wave character of the giant spikes. Because of the excessive length of computational time, we had to stick to minimum probabilities in the order of 10^{-4}, even though experimentally we could manage probabilities in the order of 10^{-7}.

To conclude, a new mechanism for rogue wave emergence has been found and experimentally verified in a multistable EDFL subject to both periodic and slow stochastic modulation applied to the diode pump laser. Rogue wave main properties of the observed laser spikes are confirmed by the wave amplitude PDF. The origin of the observed phenomenon is then the interplay between stochastic processes and deterministic nonlinear dynamics. Even if less accurate the results of numerical simulation are in good agreement with experiments. Although here we have demonstrated only the $P4$ rogue wave, a similar behavior has also been found for $P3$ and $P5$ laser pulses for other parameters.

In the future, it would be interesting to study the ocean rogue waves in the context of multistability, since coexistence of attractors, mostly alternative states related to bistability, has already been discovered in the deep ocean convection [14], atmosphere dynamics [15], and more than two different stable states have been found in the thermohaline ocean circulation [16].

The authors acknowledge CONACYT (Mexico) for the financial support through Project No. 100429 and ANUIES-ECOS Project No. M08-P02.

*apisarch@cio.mx

[1] Special Issue, Discussion & Debate: Rogue Waves – Towards a Unifying Concept? edited by N. Akhmediev and E. Pelinovsky, [Eur. Phys. J. Spec. Top. **185** (2010), http://www.springerlink.com/content/1951-6355/195/].
[2] D. R. Solli, C. Ropers, P. Koonath, and B. Jalali, Nature (London) **450**, 1054 (2007).
[3] C. Bonatto *et al.*, Phys. Rev. Lett. **107**, 053901 (2011).
[4] M. Onorato, A. R. Osborne, M. Serio, and S. Bertone, Phys. Rev. Lett. **86**, 5831 (2001); M. Onorato, A. R. Osborne, and M. Serio, *ibid.* **96**, 014503 (2006).
[5] P. A. E. M. Janssen, J. Phys. Oceanogr. **33**, 863 >(2003).
[6] B. S. White and B. Fornberg, J. Fluid Mech. **355**, 113 (1998).
[7] P. Müller, C. Garrett, and A. Osborne, Oceanography **18**, 66 (2005), ://www.tos.org/oceanography/issues/issue_archive/issue_pdfs/18_3/18.3_muller_et_al.pdf .
[8] S. Kraut, U. Feudel, and C. Grebogi, Phys. Rev. E **59**, 5253 (1999).
[9] G. Huerta-Cuellar, A. N. Pisarchik, and Y. O. Barmenkov, Phys. Rev. E **78**, 035202(R) (2008).
[10] G. Huerta-Cuellar, A. N. Pisarchik, A. V. Kir'yanov, Yu. O. Barmenkov, and J. del Valle Hernandez, Phys. Rev. E **79**, 036204 (2009).
[11] A. N. Pisarchik, Yu. O. Barmenkov, and A. V. Kir'yanov, Phys. Rev. E **68**, 066211 (2003); , IEEE J. Quantum Electron. **39**, 1567 (2003); R. J. Reategui, A. V. Kir'yanov, A. N. Pisarchik, Yu. O. Barmenkov, and N. N. Il'ichev, Laser Phys. **14**, 1277 (2004), http://www.maik.ru/full/lasphys/04/10/lasphys10_04p1277full.pdf; A. N. Pisarchik and R. Jaimes-Reátegui, Phys. Lett. A **374**, 228 (2009).

[12] A. N. Pisarchik, A. V. Kir'yanov, Yu. O. Barmenkov, and R. Jaimes-Reátegui, J. Opt. Soc. Am. B **22**, 2107 (2005).

[13] See Supplemental Material at http://link.aps.org/supplemental/10.1103/PhysRevLett.107.274101 for: Oscilloscope recording in real time demonstrating rogue waves of the period-4 pulses with high peak intensity which appear every 20–40 seconds.

[14] G. Lenderink and R. Haarsma, J. Phys. Oceanogr. **24**, 1480 (1994).

[15] M. V. Kurgansky, K. Dethloff, I. A. Pisnichenko, H. Gernandt, F.-M. Chmilevsky, and W. Jansen, J. Geophys. Res. Atmos. **101**, 4299 (1996).

[16] S. B. Power and R. Kleeman, J. Phys. Oceanogr. **23**, 1670 (1993).